JOURNAL OF MATERIALS SCIENCE 22 (1987) 557–564

Spherical particles and their surface properties

Part 4 *Spherical particles of vanadium oxide, manganese oxide and iron oxide, and their isoelectric points*

S. KITTAKA, S. SASAKI
Department of Chemistry, Faculty of Science, Okayama University of Science, 1-1 Ridaicho, Okayama 700, Japan

T. MORIMOTO
Department of Chemistry, Faculty of Science, Okayama University, Tsushima, Okayama 700, Japan

Spherical particles of transition metal oxides (vanadium oxide, manganese oxide and iron oxide) were formed by the use of O_2–H_2 flame fusion and the effect of varying raw material on the product particles was investigated. Particles ranging in size from 50 to 0.01 μm were produced simultaneously by explosive decomposition of raw material which is composed of higher valent metal ions, and melting to give $V_2O_5 \rightarrow V_2O_4 + \frac{1}{2}O_2$; $Mn_2O_3 \rightarrow 2MnO + \frac{1}{2}O_2$; and $3Fe_2O_3 \rightarrow 2Fe_3O_4 + \frac{1}{2}O_2$. During cooling from the molten state particles were reoxidized completely or partially (in the surface layer) into V_2O_5, Mn_3O_4 and Fe_2O_3, respectively, depending upon the particle size. A cavity was observed electron microscopically in the smaller V_2O_5 particles, while fine single crystal (exactly polyhedral but almost spherical) particles of Mn_3O_4 and Fe_3O_4 were obtained. The isoelectric points of spherical Mn_3O_4, Fe_3O_4 and Fe_2O_3 particles were determined to be 4.0, 5.1 and 5.1, respectively.

1. Introduction

Modern material science and technology have been developing a number of new inorganic materials which have highly functional properties such as in electronics, magnetics, mechanics and chemical reactivity. Strict characterization of raw materials is desired for such uses of materials. Recently, various mono-dispersed spherical metal oxides have been produced and utilized as raw materials for ceramics. Spherical balloons of metal oxides have become very important as heat insulators and soundproofing materials. On the other hand, it also has been well known that spherical particles play a very important role in colloid chemistry as model particles [1, 2].

The present authors have been looking for spherical particles of metal oxides with a small size, i.e. with high surface area, which is appropriate for the investigation of surface properties. For this purpose, we have tried to obtain spherical particles by O_2–H_2 flame fusion of various metal oxides [3–5], by which such amorphous or polymorphous oxides as SiO_2, TiO_2 and Al_2O_3 were easily spherulized as particles larger than a few micrometres. Smaller particles, however, less than 1 μm have not been produced even in using ultrafine raw materials smaller than 0.1 μm.

As one of the surface properties of metal oxides, the isoelectric point (IEP) or point zero charge (PZC) has been measured [6–14], but it seems that there remain controversies in assigning values to materials having a definite crystal structure and/or oxidation state of the component metal ions. As the samples investigated have been identified only through X-ray diffraction analyses, their surface structures have not been confirmed unambiguously. Together with this, most metal oxide samples treated were not spherical, so that correct electrokinetic values could not be determined by conventional methods. Thus, crystallographically well-defined and spherical metal oxide samples, which can stand rigorous theoretical treatment, seem to be desired.

The spherical particles formed by us were stable against a change in oxidation state of the metal ions at the high temperature of 2000° C. This work is concerned first with the formation of spherical particles of such transition metal oxides as vanadium oxide, manganese oxide and iron oxide, which are liable to the variation of composition at high temperatures, and then to investigate them through electron microscopy. Second, the ζ-potential and IEP of spherical particles with different sizes are determined by the use of electrophoretic mobility and streaming potential methods, which permits discussion of the data in relation with those of crystal structure.

2. Experimental procedure

2.1. Materials

2.1.1. Vanadium oxide

V-1:V_2O_5 (surface area = 5.09 $m^2 g^{-1}$) was formed by pyrolysing commercial NH_4VO_3 at 400° C for 5 h in air. V-2: V_2O_3 (5.86 $m^2 g^{-1}$) was formed by reducing V-1 at 900° C in 1 atm H_2 stream for 2 h. V-3:NH_4VO_3 was supplied by Wako Pure Chemicals (Higashiku, Osaka, Japan).

0022–2461/87 $03.00 + .12

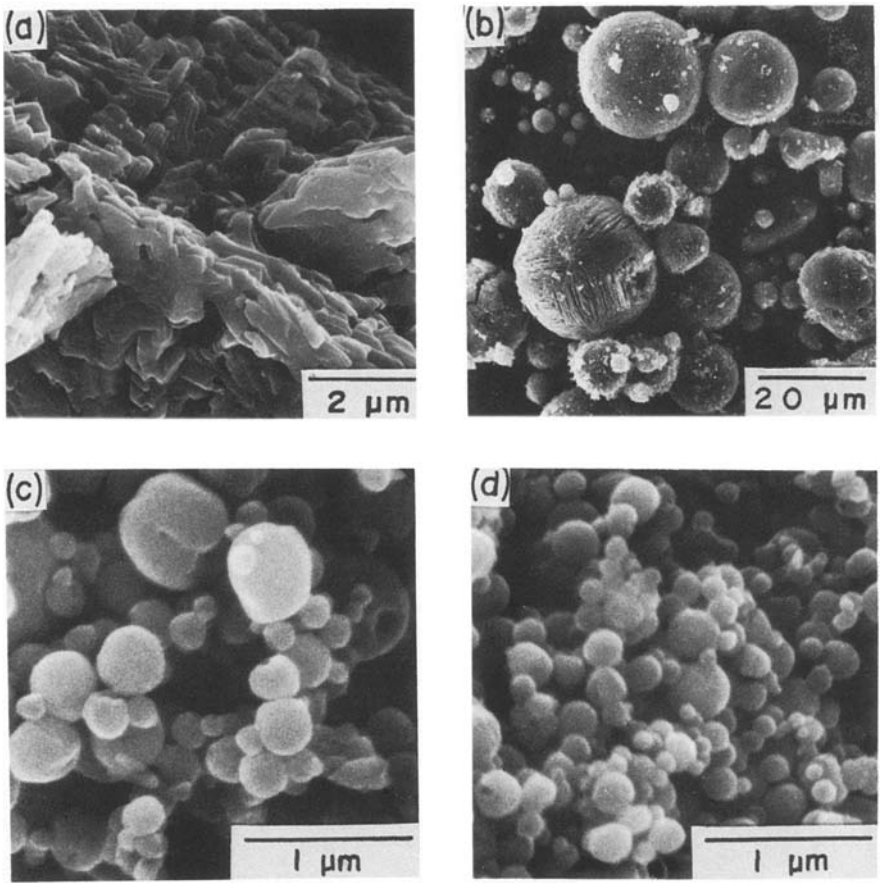

Figure 1 Electron micrographs (SEM) for vanadium oxide (V-1). (a) V_2O_5 (raw material); spheres collected at (b) D-1, (c) N, (d) G-2.

2.1.2. Manganese oxide

M-1: γ-Mn_2O_3 ($10.2\,m^2g^{-1}$) was formed by mixing 1M Mn $(NO_3)_2$ solution with ammonia water and by oxidizing the precipitate through bubbling air at room temperature. The sample was used after washing with distilled water and drying. M-2: MnO ($8.74\,m^2g^{-1}$) was formed by reducing M-1 at 400° C for 2 h in 1 atm H_2 stream. M-3: β-MnO_2 was manufactured by Alfa Products (Danvers, Massachusetts, USA).

2.1.3. Iron oxide

F-1: Fe_2O_3 ($21.8\,m^2g^{-1}$) was formed by heating hydrous iron oxide for 6 h at 600° C which was precipitated from the reaction of 1M Fe $(NO_3)_3$ with ammonia water and washed with water. F-2: Fe_3O_4 ($12.1\,m^2g^{-1}$) was formed by reducing F-1 at 400° C for 2 h in 1 atm H_2 stream. F-3: Fe_2O_3 was prepared by heating F-1 at 1200° C for 4 h in air.

2.2. Formation of particles

A set-up of O_2–H_2 flame furnace and sample collectors was the same as that used previously [3]. The diameter of the furnace is 3 cm and the length 20 cm, which is connected in series with three ducts (D-1 to D-3) of 1 m each, a stainless steel net (N), a cotton gauze (G-1), a thick cloth (G-2) and a fan. The flame was made by supplying 21 l min^{-1} H_2 and 13 l min^{-1} O_2 and the temperature was determined by use of an optical pyrometer together with a siliconit rod. The temperature in the central line of the flame of about 20 cm length from a few centimetres below the nozzle is about 2000° C and that near to the wall of the furnace about 1800° C.

2.3. Shape and crystal structure

Produced particles were investigated for their shapes electron-microscopically and for structures by X-ray diffraction. Before the SEM (JEOL JSM-35) observations, every sample was coated with Au–Pd to avoid charging-up of the samples. Particles less than 1 μm were observed by high-resolution transmission electron microscopy (HTEM) (JEOL JEM-2000EX and JEM-4000EX/AARM); particles of manganese oxide and iron oxide were spread over the carbon film which was placed over the gold-covered copper microgrid from aqueous suspension, while vanadium oxide particles were deposited from suspension with ethanol.

2.4. Electrokinetic measurements

The ζ-potential was determined by use of electrophoretic mobility (EPM) and streaming potential (SP) methods [9]. The apparatus of the former is composed of a rectangular (1 mm × 20 mm) quartz cell produced by Mitamura Riken Co. (Bunkyoku, Tokyo, Japan) and of Ag/AgCl/KCl(sat)/KNO_3(sat) agar bridge electrodes. The electric field applied was less than 10 V cm^{-1}. The mobility was determined microscopically on 10 particles in the dark field for each direction of polarization by changing the focus from the top stationary level to the bottom one. The streaming potential was determined by the use of a Takeda Riken TR 8651 (Nerimaku, Tokyo, Japan), which has a high internal impedance, and the specific conductivity of the diaphragm by a conductivity meter CM-20E manufactured by Toa Electrical Co. (Shinjukuku, Tokyo, Japan). Sample particles were suspended in 10^{-3} M KNO_3 aqueous solution one week before the

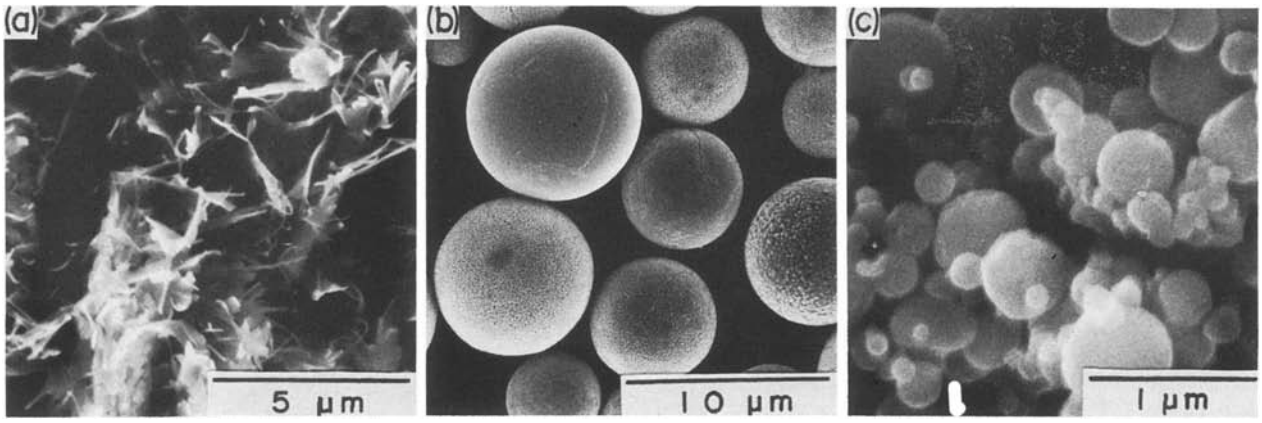

Figure 2 Electron micrographs (SEM) for vanadium oxide (V-2). (a) V_2O_3 (raw material); spheres collected at (b) D-1, (c) G-2.

measurements in order to complete the hydration of the solid surface, and the pH value was controlled by use of 10^{-3} M HNO_3 or KOH solution. The pH value of the solution was determined in the cell just after each measurement.

3. Results and discussion

3.1. Formation of spherical particles

3.1.1. Spherical particles of vanadium oxide

Fig. 1 shows a series of electron micrographs of vanadium oxide spheres formed from V_2O_5 (V-1) together with the raw material. The particle size decreases as the position for collection becomes further from the furnace, and the appearance differs markedly depending upon the collecting position. Sphericity is almost complete in the particles collected at G-1 and G-2. Most particles captured at N are somewhat large spheres, but a concave dimple can be seen on some particles. Particles collected at D-1 are very complex with a wide size distribution and various kinds of surface textures. An important fact shown here is that the G-2 particles are especially small (Fig. 1d, surface area = 12.1 $m^2 g^{-1}$) and much smaller than the starting material (Fig. 1a, 5.09 $m^2 g^{-1}$). This is the first time for the present authors to form such a small spherical particle by O_2–H_2 flame fusion [5].

Fig. 2 shows the particles from V_2O_3 (V-2). Their difference from V-1 particles can be seen in that in spite of the smaller size of the starting material, particles obtained at G-2 are somewhat larger than those from V_2O_5 and particles collected at D-1 have better sphericity but still characteristically rough surface textures. With V-3 particles (not shown here), while the starting material has much larger size of about 10 μm than that for V-1, the result is similar to that of the latter.

Fig. 3 demonstrates the X-ray diffraction analyses on V-1 spheres. There can be seen a V_2O_5 phase in all the products and a V_2O_4 phase (ASTM) in particles collected at D-1 to N. In accordance with this, the colour of the spherical particles varied from black to orange-yellow, which are characteristic of V_2O_4 and V_2O_5, respectively. A series of the same phase compositions was observed in V-3 products. In the case of V-2, however, a much larger proportion of V_2O_4 phase was obtained at D-1 compared with that of V_2O_5. This result suggests that the larger black particles having various surface textures can be assinged to be V_2O_4 and the smaller orange ones to V_2O_5.

Although the phase diagrams of vanadium oxide reported [12] is not complete for high temperature and high O_2 pressure regions, some considerations were made on the mechanism of forming spherical particles. The fact that the spherical particles collected at G-2 are smaller than the starting material of V_2O_5 can be explained by the splitting of raw material particles. This might be due to the sudden decomposition reaction

$$V_2O_5 \rightarrow V_2O_4 + \tfrac{1}{2}O_2 \qquad (1)$$

and the explosive expansion of O_2 gas (about 1.7 tonne cm^{-2}) released at high temperature (2000° C), where V_2O_4 particles are formed. Here, V_2O_4 particles formed must be molten to become droplets, although the decomposition temperature in air into V_2O_4 and its melting point have not been reported definitely. Some proportions of V_2O_4 droplets were reoxidized into V_2O_5 during cooling which should keep the liquid state down to 680° C [15], so that particles may become real spheres.

Detailed investigation of G-2 spheres through HTEM visualizes the internal structure of spheres as shown in Fig. 4 in which the surface structure does not look well defined, contrary to the expectation of the SEM picture. The first thing to be noted is that

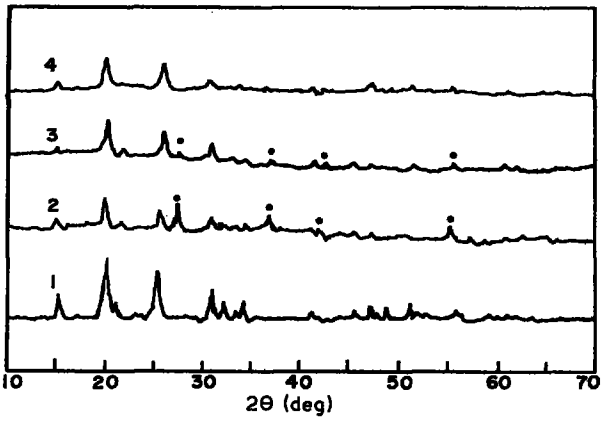

Figure 3 X-ray diffraction spectra for vanadium oxide (V-1) determined by use of Cu$K\alpha$ radiation. (1) V_2O_5 (raw material); spheres collected at (2) D-1, (3) N, (4) G-2. Peaks marked (●) are for V_2O_4 phase, others for V_2O_5 phase.

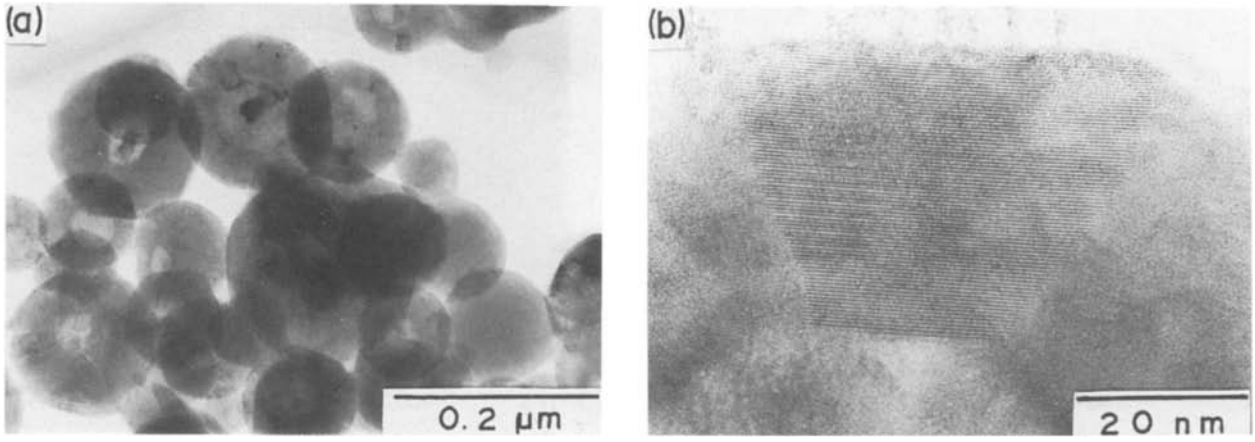

Figure 4 Electron micrographs (HTEM) for vanadium oxide (V-1) spheres collected at G-2, which were observed under different magnifications in (a) and (b).

every particle shown in Fig. 4 has a cavity inside, i.e. it constitutes a balloon, independent of the raw material. This was not found in larger particles, but they have many pores and channels inside. There are already many examples of balloons [16] of glass, aluminium oxide, etc. which are formed through various methods, e.g. by blowing the thin falling stream of molten material and passing metal hydroxide granules through the hot electric furnace. Allowing for the fact that molten V_2O_4 at 2000° C can be solidified as porous spheres, a cavity in the V_2O_5 sphere will be formed at the stage when the tiny V_2O_4 particles, which have been once solidified as porous material during cooling, are oxidized to be molten as V_2O_5 particles, giving a cavity similarly to the latter case of the above two mechanisms. A concave on some particles at N can now be explained by the appearance of the cavity, that is, the liquid state of the V_2O_5 phase is kept down to as low as 680° C so that the decrease in internal gas pressure by cooling should lead to the dragging in of some thinner part of the sheath of relatively larger fine particles. The second point is the crystallinity of particles (Fig. 4b). The size of the single-crystal domain in a particle amounts to at most the thickness of the sheath, which is somewhat smaller than the crystallite size determined by X-ray diffraction line broadening (54 nm), and gives polyhedral pictures in some particles.

Another proportion of the molten droplets was coalesced into larger spherical particles by collision in the furnace, which were crystallized mainly as V_2O_4 particles by rapid cooling. This step could be observed similarly in the experiments on V-2 where only oxidation of V_2O_3 sample occurred by the reaction

$$V_2O_3 + \tfrac{1}{2}O_2 \rightarrow V_2O_4 \qquad (2)$$

and further oxidation to V_2O_5 was very slight.

The mechanism proposed was further substantiated by the fact that raw material of explosively decomposable V_2O_5 gave plenty of particles smaller than those obtained from V_2O_3 (Fig. 5). Smaller particles were not obtained much from NH_4VO_3, although it should be explosive at high temperature through the reaction

$$2NH_4VO_3 + O_2 \rightarrow V_2O_4 + N_2 + 4H_2O \qquad (3)$$

where O_2 gas is consumed, which might inhibit the burning of H_2.

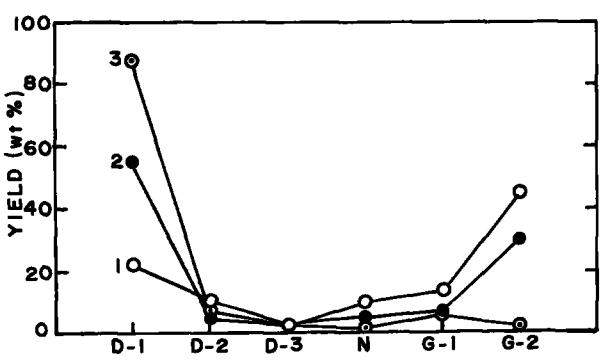

Figure 5 Yields of spherical particles of vanadium oxide as a function of collecting position. (1) V-1 (V_2O_5), (2) V-2 (V_2O_3), (3) V-3 (NH_4NO_3).

3.1.2. Spherical particles of manganese oxide

Fig. 6 shows electron micrographs of manganese oxide, γ-Mn_2O_3 (M-1), and the spherical particles collected along the flight line of the particles. The X-ray diffraction data for these particles are shown in Fig. 7. The larger particles obtained at D-1 to D-3 consist of two phases of MnO and Mn_3O_4. The content of the former decreased as the particle size did and the particles collected at positions further from N involve only the phase of Mn_3O_4. Similar morphological features were observed in the spheres from two other kinds of raw material (M-2 and M-3). The coexistence of these two phases and the phase diagram [17] depict a mechanism similar to that observed in vanadium oxide particles. γ-Mn_2O_3 was at first decomposed into MnO at high temperature by the reaction:

$$Mn_2O_3 \rightarrow 2MnO + \tfrac{1}{2}O_2 \qquad (4)$$

Some molten MnO particles were coalesced into a droplet in a flame and cooled to be oxidized into Mn_3O_4 below 1560° C from the surface through the reaction:

$$3MnO + \tfrac{1}{2}O_2 \rightarrow Mn_3O_4 \qquad (5)$$

which was completed in smaller particles. A phase Mn_2O_3 which is stable below 847° C was not observed

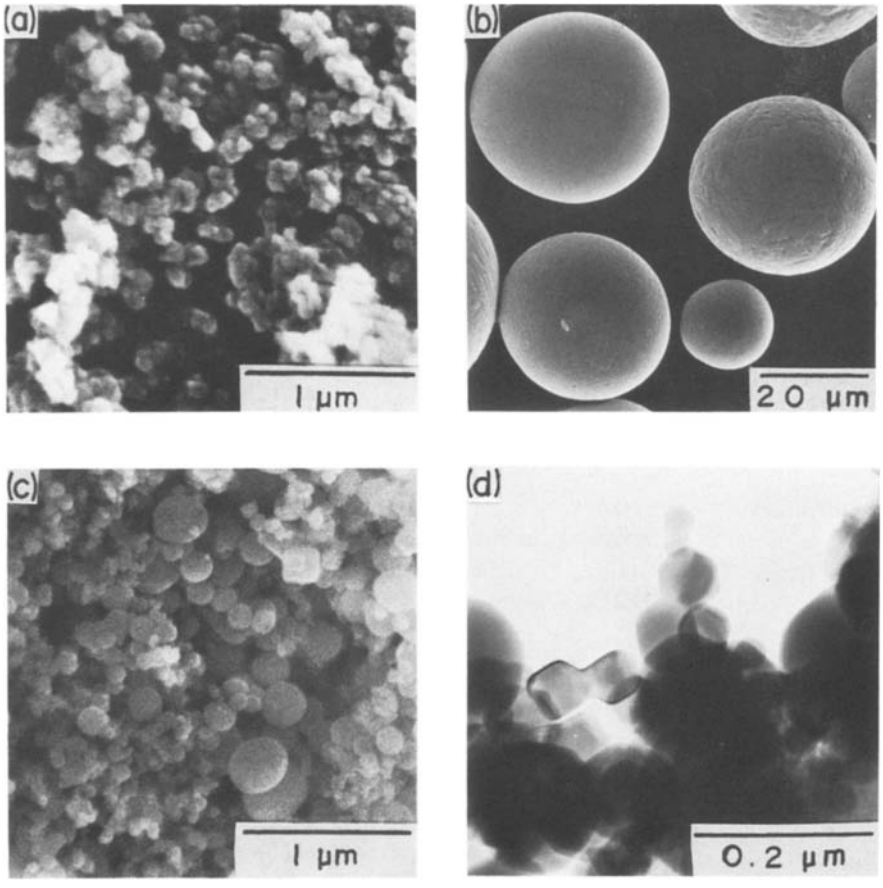

Figure 6 Electron micrographs for manganese oxide (M-1). SEM: (a) γ-Mn_2O_3 (raw material); particles collected at (b) D-1, (c) G-2. HTEM: (d) and (e) particles collected at G-2.

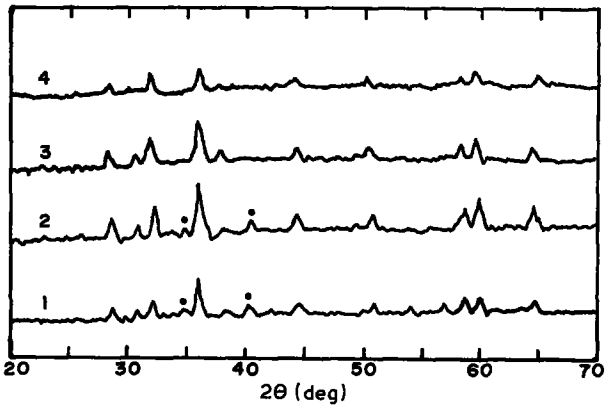

Figure 7 X-ray diffraction spectra for manganese oxide (M-1) determined by use of Cu$K\alpha$ radiation. Collecting positions: (1) D-1, (2) D-3, (3) N, (4) G-2. Peaks marked (●) are for the MnO phase, others for Mn_3O_4.

in any spherical particles by X-ray diffraction and HTEM.

HTEM observation shows that smaller particles obtained at G-2, which look spherical through SEM observations, are, as a matter of fact, polyhedral single-crystal particles (Figs 6d and e) and have a very good crystallinity as Mn_3O_4 throughout the particle. This is in contrast to the result for vanadium oxide particles which have a cavity inside. The larger particles, on the other hand, are polycrystalline spheres, which was confirmed by etching with HF solution. Fig. 8 shows the particles of β-MnO_2 as raw material with the size of about 100 μm, and spherical particles captured at G-2 formed therefrom which are much smaller than the starting material. This was caused by the explosive expansion of O_2 gas developed by a flash reaction at high temperature:

$$MnO_2 \rightarrow MnO + \tfrac{1}{2}O_2 \qquad (6)$$

In turn, if the raw material is undecomposable at a high temperature, e.g. MnO (M-3), it will not be easy to obtain such small particles. Fig. 9 demonstrates the yield of particles from three origins as a function of the distance from the furnace. The yield of largest particles for M-3, which are captured at D-1, is the most among three starting materials and that of smaller ones is the least. In contrast to M-3, the M-2 sample (MnO_2) gave the opposite dependency of the yield on the collecting position.

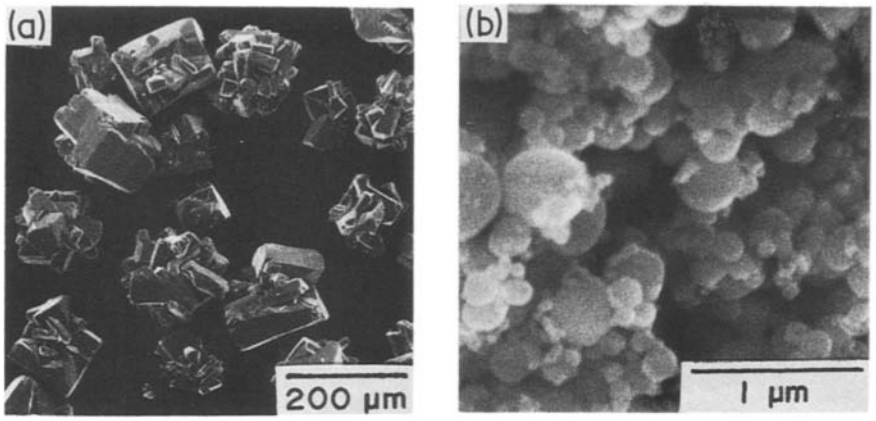

Figure 8 Electron micrographs (SEM) for manganese oxide (M-3). (a) β-MnO_2 (raw material), (b) particles collected at G-2.

3.1.3. Spherical particles of iron oxide

Fig. 10 shows a series of electron micrographs of raw material (F-1) and spheres of iron oxide. Particles obtained at any place are composed of Fe_3O_4 and an additional phase of α-Fe_2O_3 appears in the larger particles obtained at D-1 to D-3 (Fig. 11). The X-ray diffraction of particles etched by HF solution for about 6 min, by which the surface layer of the solid was completely removed, did not give the signal of Fe_2O_3 phase. Thus, the Fe_2O_3 phase in the larger particles can be assigned to the surface layer material, which might have been formed by the following reaction during cooling below 1380° C:

$$2Fe_3O_4 + \tfrac{1}{2}O_2 \rightarrow 3Fe_2O_3 \qquad (7)$$

With fine particles their crystallinity was pretty good, similarly to the ultrafine Fe_3O_4 particles produced by evaporation of iron in a low-pressure O_2 atmosphere [18]. The effect of particle size and composition of raw material on spherical particle formation was tested by using F-2 and F-3 (Fig. 12). Particles formed from Fe_3O_4 (F-2) gave a higher yield at D-1 than those from F-1. This result is similar to the relation between those for M-1 and M-3. However, with the sample of larger raw material of F-3, fine particles were not obtained as much as those expected from the case of the larger β-MnO_2. This inconsistency will be understood from the result that the larger raw material of Fe_2O_3 cannot be heated enough to be decomposed completely to Fe_3O_4. This was verified by the fact that after etching of the D-1 sample with the HF solution for 6 min only the Fe_2O_3 phase was left and detected in the remaining solid phase by X-ray diffraction. It can now be clearly concluded that the explosive decomposition of metal oxide at high temperature leads the production of fine spherical particles.

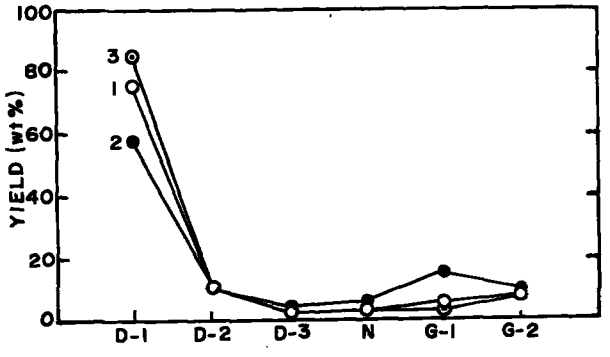

Figure 9 Yields of spherical particles of manganese oxide as a function of collecting position. (1) M-1 (γ-Mn_2O_3), (2) M-2 (MnO), (3) M-3 (β-MnO_2).

3.2. Electrification of spherical particles of manganese oxide and iron oxide

There are several reports [19–21] which determined electrokinetic values for the fine spherical particles formed mainly by precipitation, but few of the particles formed by dry methods [22]. In Figs 13a and b ζ-potential values, which were determined on the particles captured at D-1 and G-2, are plotted as a function of the pH of the solution. Here, the streaming potential method was applied to the D-1 sample and the conventional Smoluchowski equation was used for the calculation of the ζ-potential. For smaller particles collected at G-2, the electrophoretic method was utilized for ζ-potential determination with Henry's equation corrected by Overbeek [23]. The particle size was analysed through SEM photographs and thereby $\kappa a = 4.89$ was determined for manganese oxide particles and 6.9 for iron oxide particles; observations were carried out by aiming at particles with a size around 0.1 μm. The agreement between the ζ-potential values of spheres obtained at D-1 and G-2 is fairly good on each oxide particle. The IEP value of Mn_3O_4 particles determined, 3.9 to 4.3, is similar to the 3.3 to 4.0 reported by the present authors previously [12], who proposed the significance of tetrahedrally coordinated Mn^{3+} or Mn^{4+} on the electrification of manganese oxide. The agreement between the IEP values for iron oxide particles collected at G-2 and D-1 is somewhat curious because of the difference in surface structures between Fe_3O_4 and Fe_2O_3, as described before. Many data for the IEP and PZC of synthetic Fe_2O_3 are around 8.0 [6], while those of natural single-crystal particles are between 5.5 and 6.7 [6, 12], which are similar to that reported for Fe_3O_4 independently whether the materials are natural [6, 8] or synthetic [6, 10]. Thus, the D-1 particles seem to belong to the latter case; as a matter of fact, the 600° C-treated D-1 sample (Fe_2O_3) gave the same IEP value, as shown in Fig. 13b. A similar relation has also been reported for α-Al_2O_3 [6]. The present authors have found a low IEP value of 5.6 for spherical α-Al_2O_3 [24] prepared by the present method and by calcination at 1300° C.

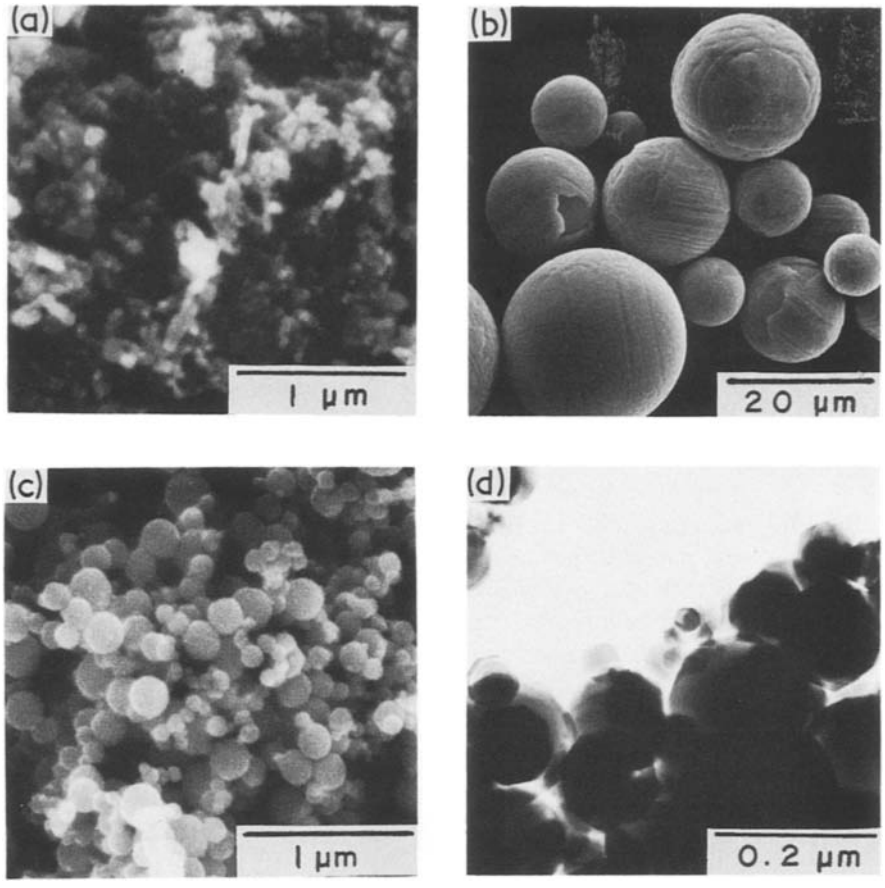

Figure 10 Electron micrographs for iron oxide (F-1). SEM: (a) Fe_2O_3 (raw material); particles collected at (b) D-1, (c) G-2. HTEM: (d) and (e) particles collected at G-2.

Our present speculation is that the particles formed through precipitation are very small in crystallite size compared to those obtained by crushing a single crystal or ingot. But, as such, the effect of crystallite size of the solid on electrification of the metal oxide surface might be serious and should be examined in detail. Although the separation of particles with a definite size was not performed, some very small particles gave very small values of ζ-potential (not shown) and those data were omitted. Details will be investigated and published.

4. Conclusions

1. Fine spherical particles of V_2O_5 were obtained by introducing V_2O_5, V_2O_3 or NH_4VO_3 into an O_2–H_2 flame, by which small V_2O_4 droplets were formed by explosive decomposition at first and oxidized by air into fine V_2O_5 particles. A small V_2O_5 particle was formed as a balloon which has a hollow surrounded by a well-crystallized sheath.

2. Fine polyhedral but almost spherical single-crystal particles of Mn_3O_4 and Fe_3O_4, were formed by the same method as used in V_2O_5 particle formation. Larger particles of Mn_3O_4 are really spherical and composed of MnO phase inside, while those of Fe_3O_4 are covered with an Fe_2O_3 layer.

3. ζ-potential and IEP values were determined on the Mn_3O_4 and Fe_3O_4 particles as a function of the pH of 10^{-3} M KNO_3 solution. The IEP for Mn_3O_4 is 3.9 to 4.3 and that for Fe_3O_4 and Fe_2O_3 5.1.

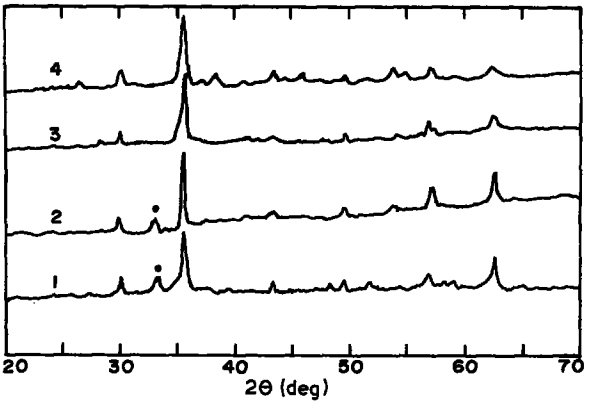

Figure 11 X-ray diffraction spectra for iron oxide (F-1) determined by use of Cu$K\alpha$ radiation. Collecting positions: (1) D-1, (2) D-3, (3) N, (4) G-2. Peaks marked (●) are for the Fe_2O_3 phase, others for Fe_3O_4.

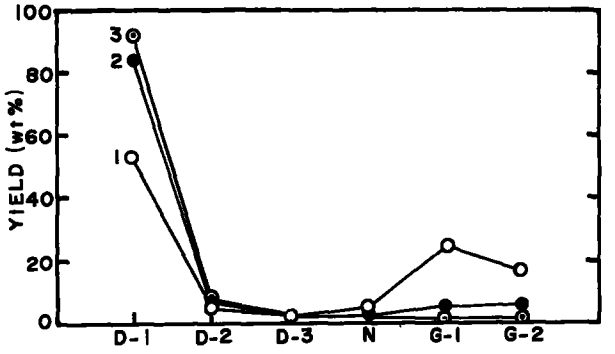

Figure 12 Yields of spherical particles of iron oxide as a function of collecting position. (1) F-1 (Fe_2O_3 prepared at 600° C), (2) F-2 (Fe_3O_4), (3) F-3 (Fe_2O_3 prepared at 1200° C).

The present method for preparing spherical particles cannot yield monodisperse particles, but on the other hand it can give particles with a variety of sizes simultaneously. Accordingly, it will be advantageous for the investigation of the effect of particle size on the physical properties of the material.

Acknowledgement

The authors express sincere thanks to Dr Yasuhiro Yokota of JEOL, who is now working at Osaka University, for his kind assistance in taking high-resolution electron micrographs.

References

1. F. K. HANSEN and E. MATIJEVIĆ, *J. Chem. Soc. Faraday I* **76** (1980) 1240.
2. S. YOSHIMURA and S. HACHISU, *Prog. Colloid Polym. Sci.* **68** (1983) 50.
3. T. MORIMOTO, T. KADOTA, H. YANAZAWA and S. KITTAKA, *Bull. Chem. Soc. Jpn* **53** (1980) 26.
4. T. MORIMOTO and S. KITTKA, *J. Colloid Interface Sci.* **78** (1980) 26.
5. S. KITTAKA and T. MORIMOTO, *Bull. Chem. Soc. Jpn* **54** (1981) 2882.
6. G. A. PARKS, *Chem. Rev.* **65** (1965) 177.
7. T. W. HEALY, A. P. HERRING and D. W. FUERSTENAU, *J. Colloid Interface Sci.* **21** (1966) 435.
8. S. M. AHMED and D. MAKSIMOV, *Can. J. Chem.* **46** (1968) 3841.
9. T. MORIMOTO and S. KITTAKA, *Bull. Chem. Soc. Jpn* **47** (1974) 1586.
10. P. TEWARI and W. LEE, *J. Colloid Interface Sci.* **52** (1975) 77.
11. W. STUMM, R. KUMMERT and L. SIGG, *Croat. Chem. Acta* **48** (1976) 491.
12. S. KITTAKA and T. MORIMOTO, *J. Colloid Interface Sci.* **75** (1980) 398.

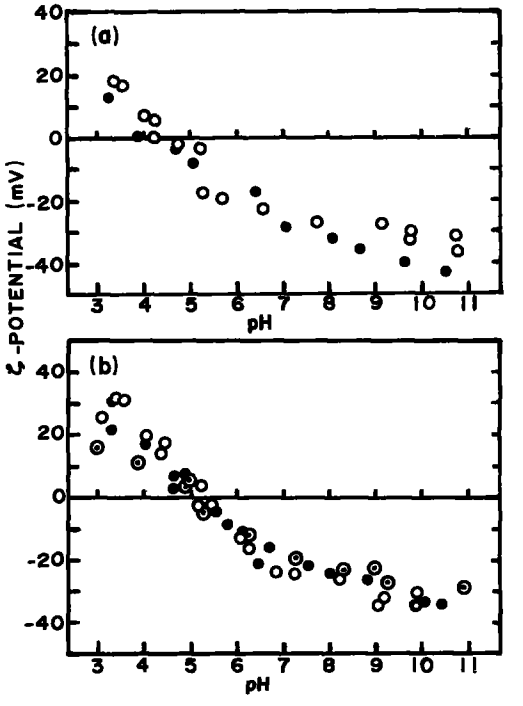

Figure 13 ζ-potential of spherical particles of (a) manganese oxide and (b) iron oxide as a function of the pH of 10^{-3} M KNO_3 solution. (○, ⊙) data determined by applying the streaming potential method on particles collected at D-1. The latter data were obtained on the sample treated at 600° C in air. (●) data determined by applying the electrophoretic method on particles collected at G-2.

13. A. E. REGAZZONI, M. A. BLESA and A. J. G. MAROTO, *ibid.* **91** (1983) 560.
14. A. HUSAIN, *ibid.* **102** (1984) 380.
15. K. KOSUGE, *J. Phys. Chem. Solids* **28** (1967) 1613.
16. S. KOIE, *Hyomen* **18** (1980) 520.
17. A. MUAN, in "High Temperature Oxides", Part 1, edited by Allen M. Alper (Academic Press, New York, 1970) p. 317.
18. M. ODA, in Proceedings of Symposium on Formation, Dispersion and Coagulation of Fine Particles and Application, Tokyo, December 1986 (Division of Colloid and Surface Chemistry of Japan Chemical Society) p. 1.
19. E. MATIJEVIĆ and P. SCHEINER, *J. Colloid Interface Sci.* **31** (1969) 257.
20. P. McFADYEN and E. MATIJEVIĆ, *J. Inorg. Nucl. Chem.* **35** (1973) 1883.
21. R. BRACE and E. MATIJEVIĆ, *ibid.* **35** (1973) 369.
22. M. VISCA and E. MATIJEVIĆ, *J. Colloid Interface Sci.* **68** (1979) 308.
23. P. W. WIERSEMA, A. L. LOEB and J. TH. G. OVERBEEK, *ibid.* **22** (1966) 178.
24. S. KITTAKA, unpublished work (1980).

Received 21 March
and accepted 5 June 1986